Breast Cancer Research

RESEARCH

Open Access

Ultrasound-based quantitative microvasculature imaging for early prediction of response to neoadjuvant chemotherapy in patients with breast cancer

Soroosh Sabeti[1], Nicholas B. Larson[2], Judy C. Boughey[3], Daniela L. Stan[4], Malvika H. Solanki[5], Robert T. Fazzio[6], Mostafa Fatemi[1] and Azra Alizad[1,6*]

Abstract

Background Angiogenic activity of cancerous breast tumors can be impacted by neoadjuvant chemotherapy (NAC), thus potentially serving as a marker for response monitoring. While different imaging modalities can aid in evaluation of tumoral vascular changes, ultrasound-based approaches are particularly suitable for clinical use due to their availability and noninvasiveness. In this paper, we make use of quantitative high-definition microvasculature imaging (qHDMI) based on contrast-free ultrasound for assessment of NAC response in breast cancer patients.

Methods Patients with invasive breast cancer recommended treatment with NAC were included in the study and ultrafast ultrasound data were acquired at pre-NAC, mid-NAC, and post-NAC time points. Data acquisitions also took place at two additional timepoints – at two and four weeks after NAC initiation in a subset of patients. Ultrasound data frames were processed within the qHDMI framework to visualize the microvasculature in and around the breast tumors. Morphological analyses on the microvasculature structure were performed to obtain 12 qHDMI biomarkers. Pathology from surgery classified response using residual cancer burden (RCB) and was used to designate patients as responders (RCB 0/I) and non-responders (RCB II/III). Distributions of imaging biomarkers across the two groups were analyzed using Wilcoxon rank-sum test. The trajectories of biomarker values over time were investigated and linear mixed effects models were used to evaluate interactions between time and group for each biomarker.

Results Of the 53 patients included in the study, 32 (60%) were responders based on their RCB status. The results of linear mixed effects model analysis showed statistically significant interactions between group and time in six out of the 12 qHDMI biomarkers, indicating differences in trends of microvascular morphological features by responder status. In particular, vessel density (p-value: 0.023), maximum tortuosity (p-value: 0.049), maximum diameter (p-value: 0.002), fractal dimension (p-value: 0.002), mean Murray's deviation (p-value: 0.034), and maximum Murray's deviation (p-value: 0.022) exhibited significantly different trends based on responder status.

*Correspondence:
Azra Alizad
Alizad.Azra@mayo.edu

Full list of author information is available at the end of the article

Conclusions We observed microvasculature changes in response to NAC in breast cancer patients using qHDMI as an objective and quantitative contrast-free ultrasound framework. These finding suggest qHDMI may be effective in identifying early response to NAC.

Keywords Breast cancer, Neoadjuvant chemotherapy, Quantitative high-definition microvasculature imaging, Ultrasound

Introduction

Neoadjuvant chemotherapy (NAC) is increasingly used in patients with breast cancer to eradicate cancer cells and assess tumor response to systemic therapy. Response information is used to guide additional systemic therapy. Complete eradication of disease (pathologic complete response, pCR) varies with breast cancer molecular subtype [1] and the majority of NAC recipients manifest some response [2–4],. pCR is associated with cancer outcomes including event-free survival as well as overall survival [5]. Monitoring and early prediction of NAC response can guide and inform timely modifications to the treatment plans and are, therefore, highly consequential [6].

Clinical assessment of NAC response is generally conducted through physical examination, and potentially using different imaging modalities including magnetic resonance imaging (MRI), mammography, and ultrasound, prior to surgery [7]. Several studies have examined the performance of these imaging modalities and research on new modes of assessment of treatment response to NAC is ongoing [8, 9].

Ultrasound is a particularly attractive imaging option for screening and response monitoring due to its accessibility, affordability, and non-invasive nature. Studies on NAC response evaluation using B-mode [10], color Doppler [11], and contrast-enhanced ultrasound [12] have shown limitations in accurately predicting pCR. More recently, the use of shear wave elastography has been investigated and shown promising results [13, 14].

Angiogenesis is considered to be an essential component in progression of tumor growth [15]. Development of complex vascular structures to feed the proliferating cancer cells is inherent to this process. Studies have shown that effective NAC administration impacts tumoral angiogenic activity [16, 17]. As a result, monitoring and analysis of the changes in vascular features of cancerous masses can provide insights and act as biomarkers for evaluation of NAC response.

Contrast-free-ultrasound-based methods for microvasculature imaging have seen rapid developments in recent years [18–20]. Recent development of the quantitative high-definition microvasculature imaging, qHDMI, introduces new imaging biomarkers that differentiate benign from malignant tumors [20–22]. Quantitative analysis of the qHDMI biomarkers has enabled differentiation of malignant lesions from their benign counterparts in different organs [19, 23–27]. The reproducibility of the proposed imaging technique has been demonstrated using different ultrasound machines, in different organs, and different operators [19, 23–28]. To evaluate and predict NAC response in breast cancer patients, some studies have employed power Doppler imaging and superb microvascular imaging (SMI) [29–31]. However, these methods generally lack structural and morphological analysis of tumor vessels, the addition of which can provide better insight into the microvascular changes caused by NAC, thus potentially facilitating early response prediction.

In this study, we utilize a contrast-free ultrasound technique named quantitative high-definition microvasculature imaging (qHDMI) for the purpose of evaluating and early prediction of breast cancer response to NAC. We derive a number of features characterizing the morphology of tumoral microvessel networks and evaluate their variations at different time points, prior to NAC commencement (pre-NAC), in the middle of the treatment duration, approximately 2 months after NAC commencement (mid-NAC), and at the end of treatment, prior to surgery (post-NAC). Additionally, we investigate the potential of our method by observing the changes in microvasculature for two additional time points, two-weeks, and one month after NAC commencement. We show how significant changes in morphological features of microvessels as early as two weeks from the outset of NAC can be detected and potentially used for prediction of response to NAC.

Methods

Study participants

A total of 53 patients with biopsy-proven invasive breast cancer recommended for treatment with neoadjuvant chemotherapy (excluding neoadjuvant endocrine therapy) were recruited for this study. The exclusion criteria involved having breast implants or prior mastectomy. The study was Institutional Review Board (IRB) approved and was compliant with the Health Insurance Portability and Accountability Act (HIPAA). All patients signed an informed consent form prior to their first data acquisition session.

Data acquisition

This was a prospective study that involved two groups of participants, based on their preference and availability.

The first group (containing 40 patients) participated in three data acquisition sessions/visits, that were scheduled before the initiation of NAC (pre-NAC / V_{PRE}), at some point (about eight weeks after the initiation) in the middle of therapy (mid-NAC / V_{MID}), and at the end of therapy (about 24 weeks after NAC initiation) before the surgery (post-NAC / V_{POST}). The second group (involving 13 patients) participated in five visits, which included the same three time points as the first group and in addition at two weeks after the initiation of NAC (2-week-NAC / V_{2Weeks}) and at one month after the initiation of NAC (one-month-NAC / V_{1Month}).

The ultrasound data acquisition for each participant during each visit was performed by one of our four experienced sonographers. A linear array transducer L3-12 H (typical frequency range 3–12 MHz) operating at a center frequency of 8.5 MHz attached to an Alpinion E-Cube 12R ultrasound system (Alpinion Medical Systems, Seoul, South Korea) was used to acquire ultrasound in-phase and quadrature (IQ) data in the plane wave imaging mode. Time gain compensation (TGC) settings were adjusted, if necessary, by the sonographers to accurately locate the lesions, and a suitable imaging plane was determined to cover the lesion in its entirety, generally in its largest cross-section. The sonographers were only involved in locating the breast lesions in B-mode ultrasound. Data acquisition (using the same machine under consistent acquisition settings) and subsequent data processing steps were performed by the investigating team. Compounded plane wave IQ data frames were acquired for a duration of 3 s at an effective frame rate of ~600 frames per second. During each acquisition, patients were instructed to pause respiration to limit motion artifacts. The lesion is likely to change shape over the course of the treatment, but the sonographers would locate the lesion at each visit using the initial clock-face position and distance from the nipple, as well as the hyperechoic biopsy clip inside the lesion.

Tumor pathology status

Estrogen receptor (ER), progesterone receptor (PR) and HER2 status were obtained from patients' pathology reports. Estrogen and progesterone receptor status was considered as positive when >1% tumor nuclei showed positive nuclear staining. HER2 status was determined by immunohistochemistry (scores of 0, 1+, 2+ and 3+) and fluorescence in-situ hybridization (FISH) was performed to check for HER2 gene application in tumors with equivocal (score 2+) staining.

Microvasculature visualization and quantification

The method for visualization of tumor microvasculature and quantification of its morphological features is what we refer to as qHDMI [20–22]. The visualization portion of the process consists of the following steps. We begin by reshaping the stack of IQ data frames into a spatio-temporal (Casorati) matrix. We then apply singular value decomposition (SVD) and spectral filters to remove tissue clutter from the data. A top-hat filter is subsequently used to detect and remove the background noise. Finally, a vessel-enhancing Hessian-based filter is employed to further accentuate the vessel-shaped structures. The denoising and vessel enhancement steps are necessary to ensure isolation of vessel structures from background noise, thereby facilitating morphological analysis of the vessels. The next step involves a manual segmentation of the lesion. Then the boundaries of the segmented lesion are dilated omnidirectionally by 2 mm. This is done to ensure inclusion of the peripheral vasculature. The 2 mm dilation is empirically selected, as the majority of the peritumoral vasculature in our data is generally observed within this range. The resulting dilated segmentation is then used as a mask to isolate the lesion and its periphery. The quantification portion of the process begins by binarizing the masked microvasculature image, followed by morphological hole-filling, opening and closing to remove noise-like structures. Subsequently, skeletonization and cleaning (spur and isolated pixels) prepare the image for morphological quantification. Through this process, 12 features/biomarkers are extracted for each image. These biomarkers include vessel density (VD), number of vessel segments (NV), number of branch points (NB), mean tortuosity as measured by the distance metric (τ_{mean}), maximum tortuosity as measured by the distance metric (τ_{max}), mean vessel diameter (D_{mean}), maximum vessel diameter (D_{max}), fractal dimension (FD), mean of Murray's deviation (MD_{mean}), maximum of Murray's deviation (MD_{max}), mean of bifurcation angle (BA_{mean}), and maximum of bifurcation angle (BA_{max}). The computation details for each of these biomarkers can be found in [21] and [19], as well as the included supplementary material. All the data processing and image processing were performed in MATLAB R2019a (Mathworks Inc., Natick, MA, USA). Microvasculature image visualization and vessel quantification in the qHDMI framework are objective processes and do not necessitate subjective interventions.

pCR label generation

Each participant was labeled as either responder or non-responder based on their residual cancer burden from the surgical pathology results [32]. The pathologists were blinded to the data and image processing and the data acquisition and processing team were blinded to the pathology. The evaluation of pCR was conducted via the residual cancer burden (RCB) metric defined as: $RCB = 1.4 \times (f_{inv} \times d_{prim})^{0.17} + [4 \times (1 - (0.75)^{LN}) \times d_{met}]^{0.17}$, where f_{inv} indicates the proportional area containing

invasive carcinoma, d_{prim} is a measure of the remaining primary tumor, LN is the number of lymph nodes involved in metastasis, and d_{met} is the diameter of the largest metastatic lymph node. Four categories are considered for RCB: RCB-0 (RCB = 0), RCB-I (0 < RCB <= 1.36), RCB-II (1.36 < RCB <= 3.28), and RCB-III (RCB > 3.28). The RCB thresholds are statistically determined to provide prognosis-based separation of classes with no residual disease (RD), minimal RD, moderate RD, and extensive RD [32]. In this study, RCB-0 and RCB-I cases were labeled as responder, while RCB-II and RCB-III cases were labeled as non-responder [33].

Statistical analysis

The values of the qHDMI biomarkers for the responder and non-responder groups were computed for each visit. A two-sided Wilcoxon rank-sum test was performed to compare the distributions of the biomarkers at each visit. Biomarker trajectories over time were analyzed using linear mixed effects models to account for intra-individual correlation, modeling the effects of responder status for individual biomarkers treating time as a continuously valued predictor and thus assuming a linear function of time. Random intercepts were applied and differences in trajectories by responder status were tested by including a time interaction with responder status, resulting in the model form $Y_{ij} = \beta_0 + \beta_1 t_j + \beta_2 X_i + \beta_2 t_j X_i + z_i + ?_{ij}$ where Y_{ij} represents the biomarker value at timepoint t_j for participant i, X_i is the binary responder status for participant i, z_i is the random intercept effect, and $?_{ij}$ is the residual error. Model assumptions, such as variance homogeneity and linearity, were assessed and potential transformations of the biomarker values were considered, as appropriate. In all cases, a p-value<0.05 was considered statistically significant. All statistical analyses were performed in R version 4.4.1 (R Core Team, Vienna, Austria) using RStudio (RStudio, PBC, Boston, MA).

Sample size

This study was designed with the expectation of a 70% chemotherapy response rate among the target patient population. Targeting 80% power to identify a 1 SD mean difference between qHDMI biomarkers by response status at a given timepoint, a total of 39 patients would be necessary when performing a two-sample Student's t-test under a two-sided hypothesis and an alpha level of 0.05. No adjustments were made to the alpha level for multiple testing based on high expected correlation among qHDMI biomarkers. To account for potential participant drop-out over time, a 20% sample size inflation factor was considered for total enrollment, resulting in a target sample size of 50 patients. Analyses that leverage repeated longitudinal measures should only have increased statistical power.

Results

Out of the 53 patients included in the study, 32 (60%) were responders (RCB 0/I) and 21 (40%) were non-responders (RCB II/III).

There were missing data for some of the visits among the participants. These were either due to patients not showing up for their visits or failures of the data acquisition system and were considered missing completely at random. Figure 1 shows the number of available samples for each visit of the two groups of participants.

Table 1 summarizes the age and pathology results for these two groups of patients. Among the 40 patients in the 3-Visit group, 20 were responders and 20 were non-responders. While among the 13 patients in the 5-Visit group, 12 were responders and 1 was non-responder. The

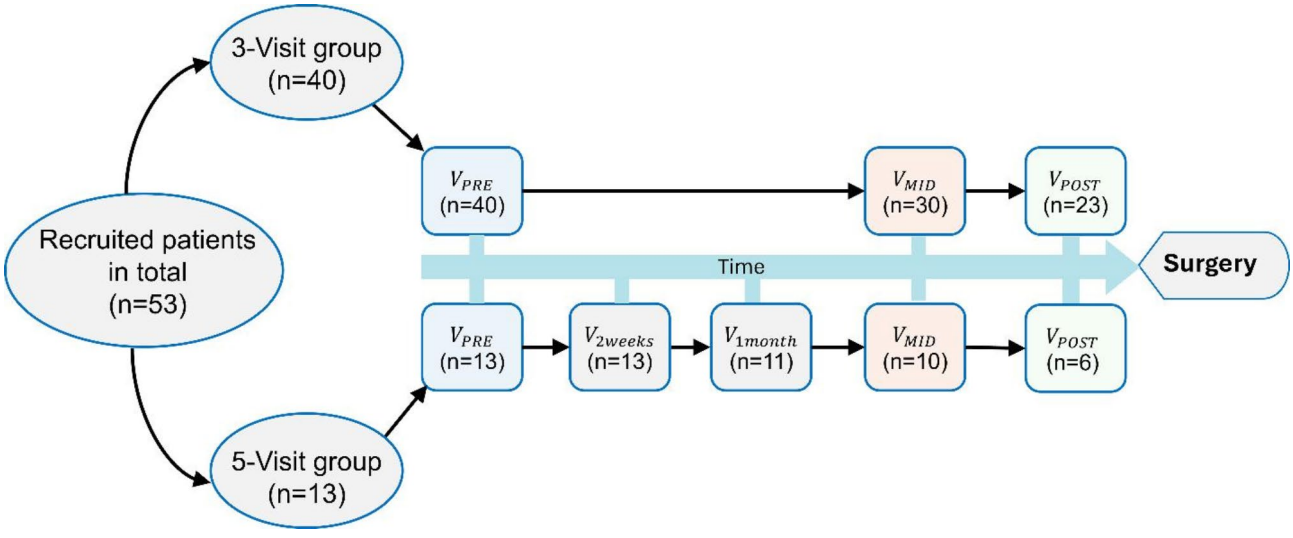

Fig. 1 The number of participants and available data acquisitions for each visit

Table 1 Age and pathology results for the two groups of patients

Parameters	Responder ($n=32$)	Non-responder ($n=21$)	Overall ($n=53$)
Age (mean ± standard deviation)	51.6 ± 12.7	55.6 ± 12.6	53.2 ± 13.1
Pathologic type			
Invasive ductal carcinoma	28 (88%)	17 (81%)	45 (85%)
Invasive lobular carcinoma	2 (6%)	1 (5%)	3 (6%)
Invasive mammary carcinoma with mixed ductal and lobular features	2 (6%)	3 (14%)	5 (9%)
Pathologic grade			
I/II	9 (28%)	11 (52%)	20 (38%)
III	23 (72%)	10 (48%)	33 (62%)
Estrogen receptor status			
Positive	16 (50%)	17 (81%)	33 (62%)
Negative	16 (50%)	4 (19%)	20 (38%)
Progesterone receptor status			
Positive	12 (37%)	15 (71%)	27 (51%)
Negative	20 (63%)	6 (29%)	26 (49%)
HER2 status			
Positive	11 (34%)	2 (10%)	13 (25%)
Negative	21 (66%)	19 (90%)	40 (75%)

distribution of the qHDMI biomarkers for the responders and non-responders for different visits are reported in Table 2. P-values are obtained using the Wilcoxon rank-sum test.

Figures 2 and 3 show example qHDMI results for the pre-chemotherapy (V_{PRE}), mid-chemotherapy (V_{MID}), and post-chemotherapy (V_{POST}), of a patient in the responder group, and one in the non-responder group, respectively. It can be observed that for the responder patient, the malignant tumor before the initiation of therapy has dense and complex microvascular structure. However, along with the decrease in size, tumor vascularity and vascular irregularity appears to decline significantly in the middle of therapy and remain low at the end of the therapy. These observations are reflected in the changes in qHMDI biomarker values. In particular, variations of number of vessel segments NV, maximum tortuosity τ_{max}, and maximum Murray's deviation MD_{max} over time for the patients (as shown in the pre-mid-post plots in 2 and 3) indicate a downward trend in microvascular density, structural organization, and branching anomalies for the responder case, as opposed to the non-responder patient.

Figures 4 and 5 show example qHDMI results for the pre-chemotherapy (V_{PRE}), two weeks after chemotherapy (V_{2weeks}), and one month after chemotherapy (V_{1month}), of a patient in the responder group, and one in the non-responder group, respectively. The results indicate a reduction in microvascular complexity for the responder, while the lesion vascularity retains or even experiences an increase in its relative density and

Table 2 Distribution of biomarker values (reported as mean ± standard deviation) for pre-NAC, mid-NAC and post-NAC visits (distributions of $\mathrm{V_{2Weeks}}$ and $\mathrm{V_{1Month}}$ are not reported as there is only one sample for the non-responder group for these visits)

Sample counts	Responder	Non-responder	
V_{PRE}	32	21	
V_{2Weeks}	12	1	
V_{1Month}	10	1	
V_{MID}	25	15	
V_{POST}	18	11	
Biomarkers	**Responder**	**Non-responder**	**P-value**
VD			
V_{PRE}	0.0041 ± 0.0023	0.0037 ± 0.0022	0.39
V_{MID}	0.0016 ± 0.0010	0.0024 ± 0.0015	0.10
V_{POST}	0.0009 ± 0.0009	0.0023 ± 0.0016	0.014*
NV			
V_{PRE}	41.09 ± 39.90	44.76 ± 35.05	0.58
V_{MID}	12.4 ± 9.63	16.73 ± 11.07	0.22
V_{POST}	4.83 ± 4.99	22.72 ± 13.14	0.0004*
NB			
V_{PRE}	16.34 ± 19.74	18.14 ± 16.37	0.47
V_{MID}	4.48 ± 3.79	6.26 ± 4.39	0.20
V_{POST}	1.66 ± 2.80	8.45 ± 5.00	0.0008*
τ_{mean}			
V_{PRE}	1.04 ± 0.01	1.03 ± 0.01	0.31
V_{MID}	1.03 ± 0.02	1.04 ± 0.03	0.13
V_{POST}	1.02 ± 0.01	1.03 ± 0.02	0.45
τ_{max}			
V_{PRE}	1.34 ± 0.30	1.29 ± 0.21	0.60
V_{MID}	1.15 ± 0.13	1.22 ± 0.19	0.10
V_{POST}	1.06 ± 0.04	1.22 ± 0.15	0.0039*
D_{mean} (μm)			
V_{PRE}	509.04 ± 99.35	472.80 ± 92.87	0.17
V_{MID}	490.22 ± 92.79	473.35 ± 48.85	0.89
V_{POST}	434.26 ± 89.74	446.38 ± 51.02	0.57
D_{max} (μm)			
V_{PRE}	837.84 ± 226.47	781.21 ± 187.03	0.54
V_{MID}	640.07 ± 340.30	712.83 ± 122.77	0.55
V_{POST}	449.08 ± 247.14	762.12 ± 173.19	0.0037*
FD			
V_{PRE}	1.32 ± 0.14	1.32 ± 0.11	0.76
V_{MID}	1.12 ± 0.22	1.22 ± 0.09	0.21
V_{POST}	1.03 ± 0.15	1.23 ± 0.12	0.0018*
MD_{mean}			
V_{PRE}	0.31 ± 0.08	0.30 ± 0.10	0.56
V_{MID}	0.27 ± 0.11	0.30 ± 0.07	0.56
V_{POST}	0.28 ± 0.18	0.38 ± 0.09	0.35
MD_{max}			
V_{PRE}	0.66 ± 0.25	0.65 ± 0.28	0.85
V_{MID}	0.49 ± 0.23	0.57 ± 0.14	0.24
V_{POST}	0.45 ± 0.31	0.74 ± 0.27	0.14
BA_{mean}			
V_{PRE}	100.81 ± 7.44	102.86 ± 10.38	0.72
V_{MID}	103.28 ± 13.78	105.97 ± 15.72	0.52
V_{POST}	97.17 ± 18.50	104.75 ± 14.68	0.53
BA_{max}			
V_{PRE}	141.53 ± 19.57	149.53 ± 24.60	0.10
V_{MID}	136.23 ± 23.62	133.98 ± 25.86	0.98
V_{POST}	111.39 ± 25.85	143.24 ± 16.32	0.024*

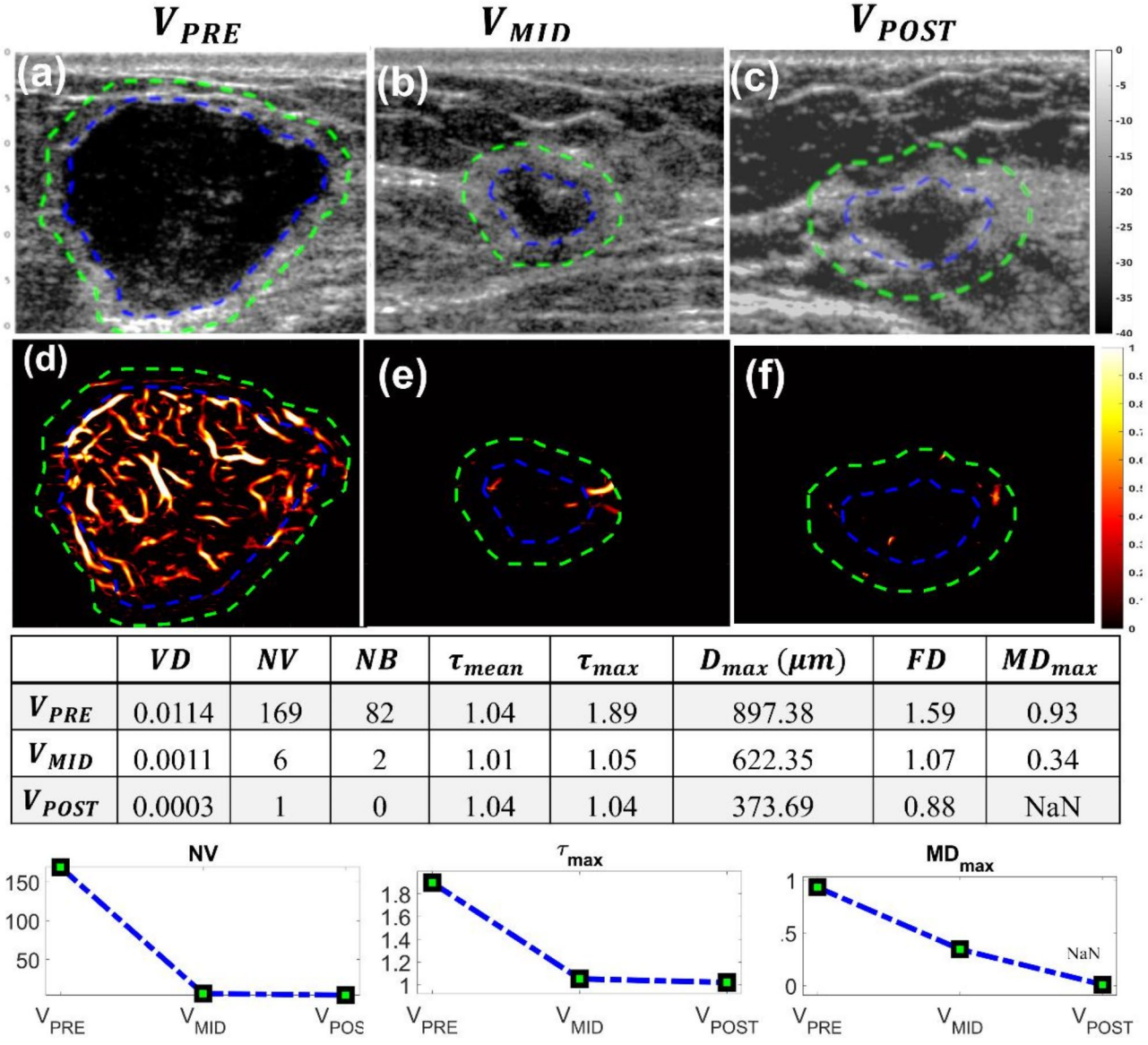

	VD	NV	NB	τ_{mean}	τ_{max}	D_{max} (μm)	FD	MD_{max}
V_{PRE}	0.0114	169	82	1.04	1.89	897.38	1.59	0.93
V_{MID}	0.0011	6	2	1.01	1.05	622.35	1.07	0.34
V_{POST}	0.0003	1	0	1.04	1.04	373.69	0.88	NaN

Fig. 2 qHDMI images, quantitative biomarkers and trend plots in a 36-year-old patient with breast cancer in the responder group. **(a**, **b**,**c)** Research B-mode US and **(d**, **e**,**f)** qHDMI images for their visits: **(a**, **d)** pre-chemotherapy, **(b**, **e)** mid-chemotherapy and **(c**, **f)** post-chemotherapy visits. Dashed blue and green curves are the segmented lesion boundaries before and after 2 mm dilation, respectively. Table under the images contains a selected set of qHDMI biomarkers calculated from the microvascular structure derived from the qHDMI images. The pre-mid-post plots represent trajectories of three of the biomarkers (NV, τ_{max}, MD_{max}) over time for this patient in the responder group

complexity for the non-responder. These variations are also reflected in the qHDMI biomarkers. The pre-mid-post plots shown in Figs. 4 and 5 manifest the trends in three of the biomarkers indicating differences in variations of microvessel complexity and branching irregularity.

The results of the linear mixed modeling of biomarker trajectories by responder status are presented in Table 3. After assessing biomarker distributions through initial model fits, the square-root transformation was applied to the values for four biomarkers (VD, NV, NB, τ_{max}). Remaining biomarkers were analyzed on the observed scale. In six of the biomarkers a statistically significant (p-value < 0.05) interaction between time and response status is observed, indicating a significant difference in variation trajectories between the responder and non-responder patients.

Figure 6. Trend plots for all of the 12 qHDMI biomarkers for V_{PRE}, V_{MID} (after ~8 weeks) and V_{POST} (after ~24 weeks). The cyan lines correspond to the responder group and the red lines correspond to the non-responder group. The error bars indicate the confidence interval across the mean values of each biomarker.

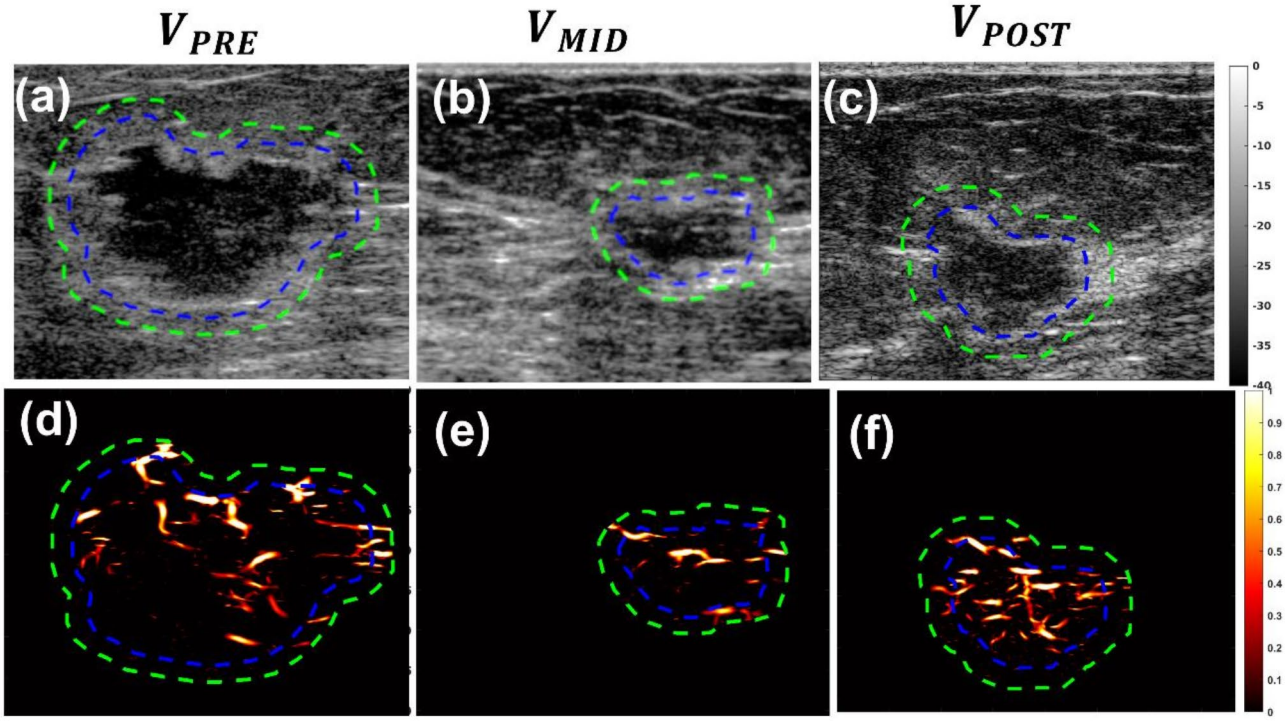

	VD	NV	NB	τ_{mean}	τ_{max}	D_{max} (μm)	FD	MD_{max}
V_{PRE}	0.0039	39	12	1.035	1.678	1201.2	1.30	0.48
V_{MID}	0.0032	12	5	1.024	1.074	892.2	1.20	0.79
V_{POST}	0.0055	33	8	1.037	1.265	693.45	1.30	0.71

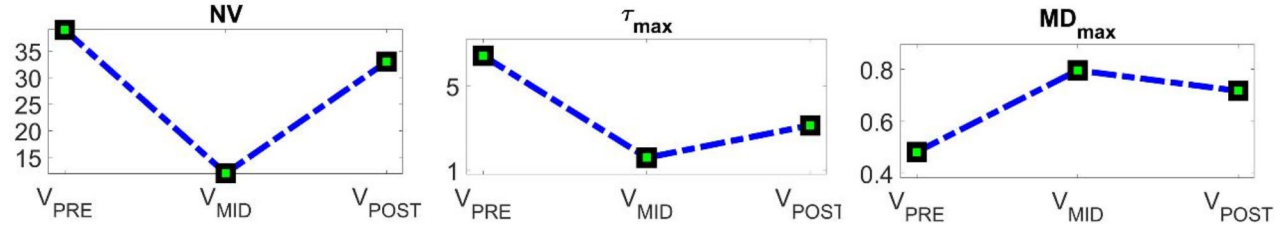

Fig. 3 qHDMI images and quantitative biomarkers and trend plots in a 74-year-old patient in the non-responder group. **(a**, **b**,**c)** Research B-mode US and **(d**, **e**,**f)** qHDMI microvasculature images for their visits: **(a**, **d)** pre-chemotherapy, **(b**, **e)** mid-chemotherapy and **(c**, **f)** post-chemotherapy visits. Dashed blue and green curves are the segmented lesion boundaries before and after 2 mm dilation, respectively. Table under the images contains a selected set of qHDMI biomarkers calculated from the microvascular structure in the image. The pre-mid-post plots represent the variations of three of the biomarkers (NV, τ_{max}, MD_{max}) over time for this patient in the non-responder group

Discussion

In this study we investigated the utility of qHDMI biomarkers in evaluating the response to neoadjuvant chemotherapy in breast cancers. Patients were classified as responders or non-responders based on their surgical pathology results and residual cancer burden. The two groups generally exhibited distinct trends in biomarker values over the course of treatment.

NAC as a systemic treatment strategy for breast cancer is administered with the goal of optimizing the systemic therapy, downstaging the tumor and facilitating the conditions for surgical interventions. Studies suggest that NAC has an impact on the angiogenic activity of tumor [34], thereby hindering further tumor development. Besides the overall tumor size reduction, not only can intratumoral vascular proliferation be affected, the vascular architecture and complexity can vary as a response to NAC [35]. The biomarkers of the qHDMI framework characterize the morphological structure of microvessels in the tumor. Observing the distribution means of these biomarkers, suggest that the vascularity level and complexity varies over the different visits as a response to

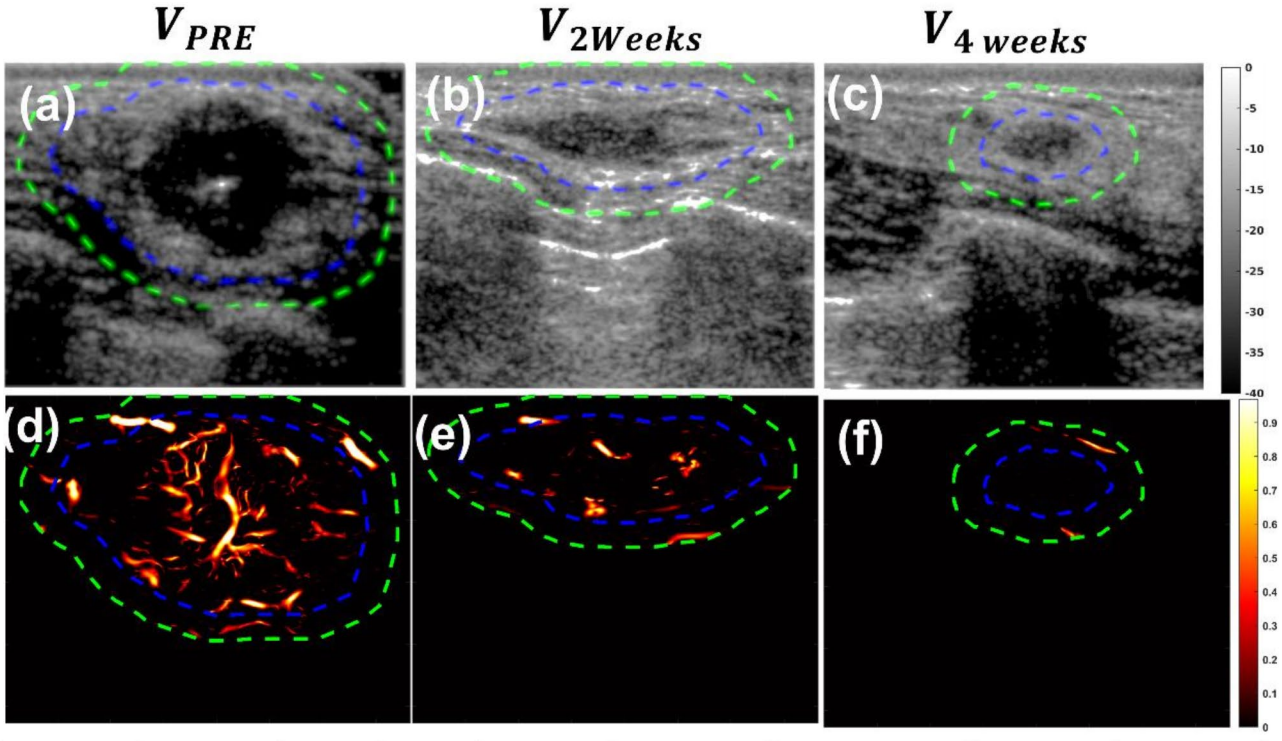

	VD	NV	NB	τ_{mean}	τ_{max}	$D_{max}\,(\mu m)$	FD	MD_{max}
V_{PRE}	0.0060	67	28	1.041	1.305	783.1	1.468	0.758
V_{2Weeks}	0.0015	9	3	1.029	1.144	849.6	1.210	0.429
V_{1Month}	0.0011	2	0	1.023	1.041	352.6	0.972	NaN

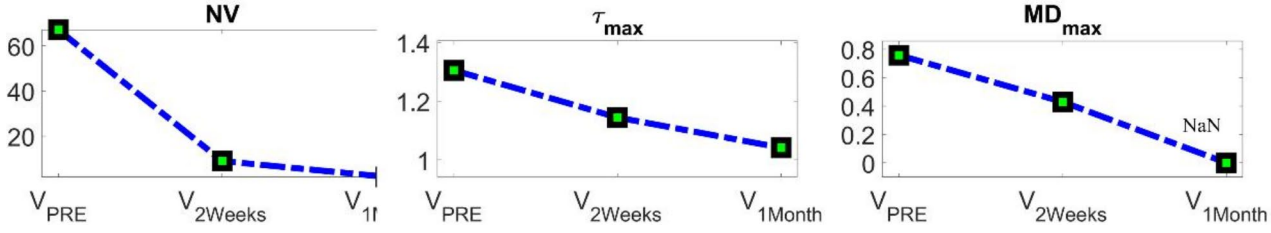

Fig. 4 qHDMI images, and quantitative biomarkers and trend plots in a 53-year-old patient in the responder group. **(a**, **b**,**c)** research B-mode US and **(d**, **e**,**f)** qHDMI microvasculature images for their visits: **(a**, **d)** pre-chemotherapy, **(b**, **e)** 2 weeks after, and **(c**, **f)** 1 month after the initiation of chemotherapy. Dashed blue and green curves are the segmented lesion boundaries before and after 2 mm dilation, respectively. Table under the images contains a selected set of qHDMI biomarkers calculated from the microvascular structure in the image. The pre-mid-post plots represent the variations of three of the biomarkers (NV, τ_{max}, MD_{max}) over time for this patient in the responder group

the treatment. While ultrasound-based studies for NAC treatment monitoring through microvasculature imaging are limited in the literature, they generally are in combination with elastography and do not involve morphological analysis of the microvessels [30, 31].

It can take several weeks for the effects of the treatment to manifest themselves in the characteristics of the tumor. Previous studies suggest that the differences in tumoral features such as elasticity and mass characteristic frequency and the predictive power of these biomarkers increase as we get closer to the mid-therapy time point [14]. In this study, we observed that, for most biomarkers, the distributional differences between the responders and non-responders became more significant with the progression of the treatment. While the decline in morphological complexity of vascular networks was captured by the qHMDI biomarkers, sample size limitations with only one non-responder participant in the 5-Visit group precluded distributional comparisons.

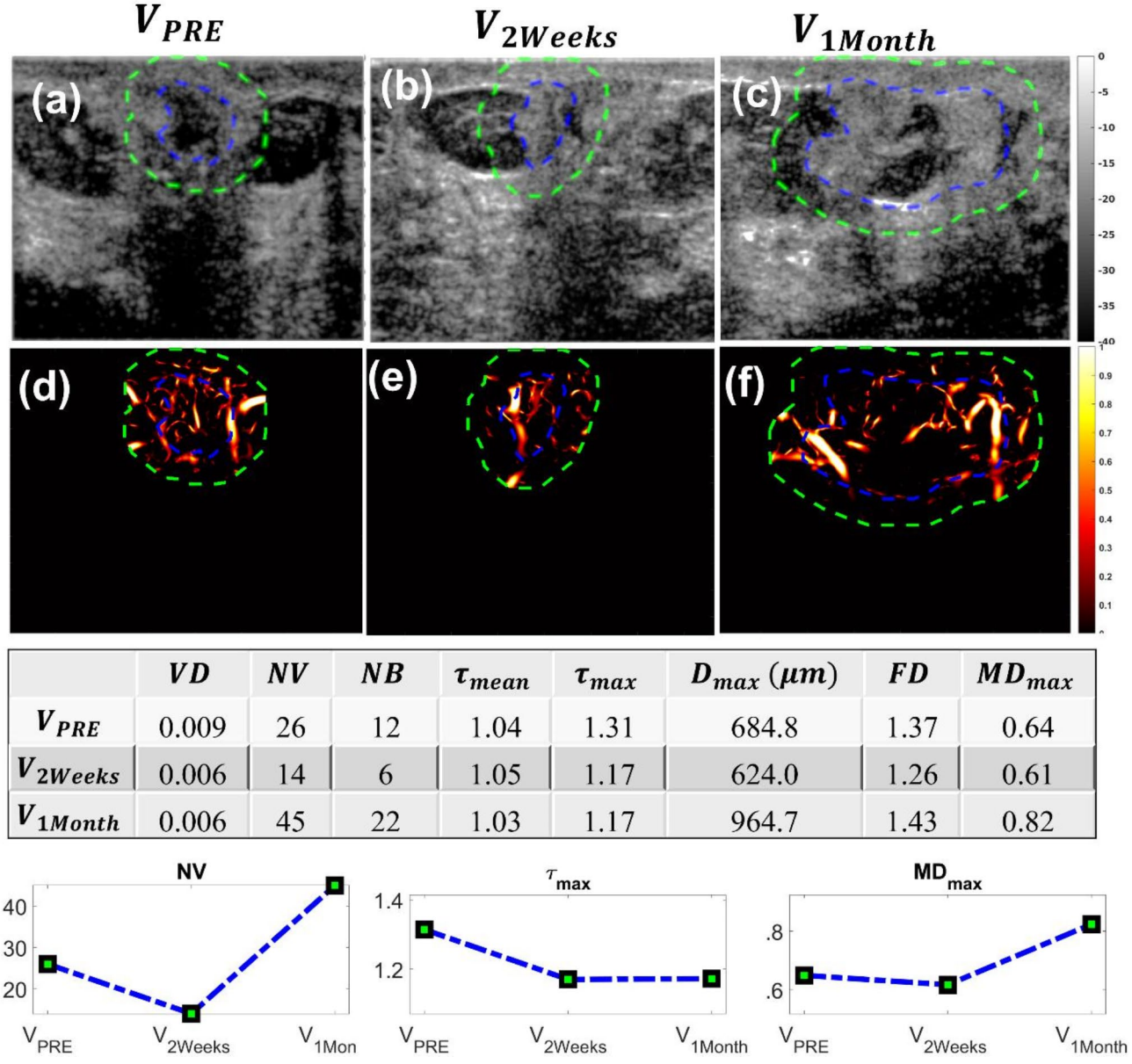

	VD	NV	NB	τ_{mean}	τ_{max}	D_{max} (μm)	FD	MD_{max}
V_{PRE}	0.009	26	12	1.04	1.31	684.8	1.37	0.64
V_{2Weeks}	0.006	14	6	1.05	1.17	624.0	1.26	0.61
V_{1Month}	0.006	45	22	1.03	1.17	964.7	1.43	0.82

Fig. 5 qHDMI images, and quantitative biomarkers and trend plots in a 49-year-old patient in the non-responder group. **(a**, **b**,**c)** research B-mode US and qHDMI microvasculature images (d, e,f) for their visits: **(a**, **f)** pre-chemotherapy, **(b**, **e)** 2 weeks after, and **(c**, **f)** 1 month after the initiation of chemotherapy. Dashed blue and green curves are the segmented lesion boundaries before and after 2 mm dilation, respectively. Table under the figures contains a selected set of qHDMI biomarkers calculated from the microvascular structure in the image. The pre-mid-post plots represent the variations of three of the biomarkers (NV, τ_{max}, MD_{max}) over time for this patient in the non-responder group

Representative responder and non-responder examples show how qHDMI biomarkers can capture microvasculature variation trends. While hypervascular tumors before the initiation of therapy may exist within the responder group, the changes in microvascular structure of the tumor can evidence the extent of the response. This can happen despite relative changes in tumor size, indicating that tumor size per se may not be a sufficient indicator of response to therapy. Similarly, we observed that changes in microvasculature can happen in as early as 2 to 4 weeks from the initiation of therapy, and while a responder case may present with a quick drop in vascularity, a non-responder case may retain or experience higher vascular complexity at these early stages.

Longitudinal analysis of the qHDMI biomarker trajectories showed that for several biomarkers, there is evidence that response over time varies significantly according to the response status of the participants. The trend plots show how there is a noticeable difference in variations of most of the biomarkers for the two groups,

Table 3 Results of mixed effects model analysis of trajectory differences by responder status for biomarkers. Bold font p-values indicate statistical significance (p-value < 0.05). (SE: standard error)

Biomarker	Estimate	SE	*P*-value
VD	-0.0007	0.0003	**0.023**
NV	-0.069	0.038	0.071
NB	-0.043	0.029	0.135
τ_{mean}	-0.006	0.004	0.149
τ_{max}	-0.009	0.004	**0.049**
D_{mean}	-3.899	2.251	0.086
D_{max}	-12.155	3.867	**0.002**
FD	-0.011	0.004	**0.002**
MD_{mean}	-0.005	0.002	**0.034**
MD_{max}	-0.013	0.005	**0.022**
BA_{mean}	-0.124	0.316	0.695
BA_{max}	-0.850	0.528	0.111

even for those biomarkers not showing a statistically significant time and group interaction. These plots also show how responder cases may have higher vascular density or tortuosity before the therapy, but how these values decrease over time relative to those of the non-responder cases.

This study has limitations. Firstly, the small sample size was restrictive for the statistical power of the tests in the study. This additionally precluded comprehensive examination of confounding effects of baseline patient and tumor characteristics on qHDMI biomarker trajectories as well as assessing the utility of baseline values on prediction of NAC treatment response after accounting for established risk factors. In future, a large-scale multicenter study is warranted to determine the generalizability and clinical utility of the method. Additionally, not all patients completed all their visits, limiting the ability to characterize trends for the biomarkers with fine granularity and precision.

The primary objective of this study was to investigate the efficacy of qHDMI in predicting the response of cancerous breast lesions to NAC in general. The effect of different NAC regimens and other types of therapy could be subject for future research. Moreover, this study was focused on two-dimensional microvasculature imaging where only one slice of the tumor was targeted for analysis. Considering the potential changes in shape and location of the tumor over the course of treatment, it was difficult to maintain a consistent slice across different

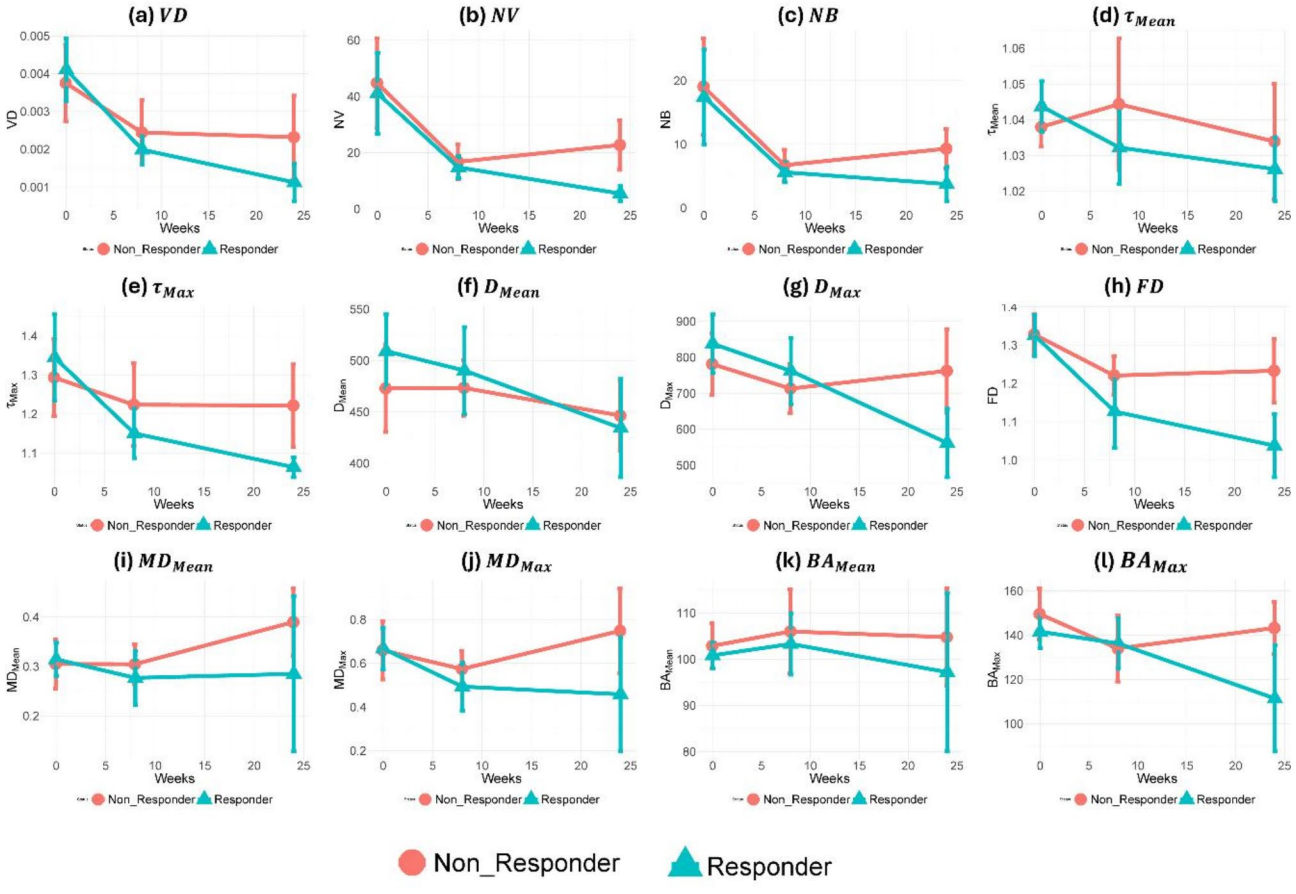

Fig. 6 shows the trend in all of the biomarkers over time for the responder and non-responder patients

visits. This is an inherent issue with two-dimensional ultrasound imaging. Future studies will involve volumetric imaging of the tumors which would provide better insights into microvascular changes with NAC. The qHDMI framework can be implemented on any ultrasound platform capable of high-frame-rate plane-wave imaging.

Conclusion

In this paper, we presented the application of a contrast-free ultrasound microvasculature imaging technique called qHDMI for early prediction of breast cancer response to neoadjuvant chemotherapy. The qHDMI biomarkers capturing morphological features of tumoral vasculature were able to detect trends in response to chemotherapy within a few weeks from the therapy initiation. Statistical analyses on the qHDMI biomarker trends showed differences between the patients responding to the therapy and those not responding. Future work could include conducting the study on a larger set of patients with additional time points/visits to achieve more reliable statistical results and the use of volumetric microvasculature imaging, enabling a more thorough analysis of tumoral microvasculature, for response prediction.

Abbreviations

qHDMI	Quantitative high-definition microvasculature imaging
ROC	Receiver operating characteristic
AUC	Area under the curve
pCR	Pathologic complete response
NAC	Neoadjuvant chemotherapy

Supplementary Information

The online version contains supplementary material available at https://doi.org/10.1186/s13058-025-01978-y.

Supplementary Material 1

Acknowledgements

The authors would like to thank all the past and present members, sonographers, and study coordinators who helped for a period of time during the years of this study.

Author contributions

Azra Alizad: Conceptualization & design, Methodology, Investigation, Visualization, Interpretation, Validation, Administrative, Resources, Funding, Supervision, Critical review, and Editing. Mostafa Fatemi: Conceptualization & design, Methodology, Investigation, Visualization, Interpretation, Validation, Administrative, Resources, Funding, Supervision, Critical review and editing. Soroosh Sabeti: Visualization, Interpretation, Investigation, Statistical analysis, Validation, Writing the original draft, Critical review and Editing Robert T. Fazzio: Visualization, Validation, Critical review and Editing. Nicholas B. Larson: Statistical methods, Formal analysis, Critical review, and Editing. Judy C Boughey Validation, Critical review and Editing. Daniela L Stan: Validation, Critical review and Editing. Malvika H Solanki: Validation, Critical review and Editing.

Funding

This work was supported in part by the NIH Grants R01CA239548 (A. Alizad and M. Fatemi), The content is solely the responsibility of the authors and does not necessarily represent the official views of NIH. The NIH did not have any additional role in the study design, data collection and analysis, decision to publish or preparation of the manuscript.

Data availability

The data that support the findings of this study are available from the corresponding author upon reasonable request. The requested data may include figures that have associated raw data. Because the study was conducted on human volunteers, the release of patient data may be restricted by Mayo policy and needs special request. The request can be sent to: Karen A. Hartman, MSN, CHRC| Administrator - Research Compliance| Integrity and Compliance Office| Assistant Professor of Health Care Administration, Mayo Clinic College of Medicine & Science| 507-538-5238| Administrative Assistant: 507-266-6286| hartman.karen@mayo.edu Mayo Clinic| 200 First Street SW| Rochester, MN 55905| mayoclinic.org. We do not have publicly available Accession codes, unique identifiers, or web links.

Declarations

Ethical approval

The Research involved human participants. The study received institutional review board approval (IRB#: 19-003028 and IRB#: 1200329) and was Health Insurance Portability and Accountability Act (HIPAA) compliant. All procedures performed in this study were in accordance with the ethical standards of the institutional and/or national research committee and with the 1964 Helsinki declaration and its later amendments or comparable ethical standards.

Informed consent

Signed IRB approved informed consent with permission for publication was obtained from all individual participants included in the study.

Competing interests

The authors declare no competing interests.

Author details

[1]Department of Physiology and Biomedical Engineering, Mayo Clinic College of Medicine and Science, Rochester, MN 55905, USA
[2]Department of Quantitative Health Sciences, Mayo Clinic College of Medicine and Science, Rochester, MN 55905, USA
[3]Division of Breast and Melanoma Surgical Oncology, Department of Surgery, Mayo Clinic College of Medicine and Science, Rochester, MN 55905, USA
[4]Department of Medicine, Mayo Clinic College of Medicine and Science, Rochester, MN 55905, USA
[5]Department of Laboratory Medicine and Pathology, Mayo Clinic College of Medicine and Science, Rochester, MN 55905, USA
[6]Department of Radiology, Mayo Clinic College of Medicine and Science, 200 1st Street SW, Rochester, MN 55905, USA

Received: 9 December 2024 / Accepted: 6 February 2025
Published online: 17 February 2025

References

1. Asaoka M, et al. Neoadjuvant chemotherapy for breast cancer: past, present, and future. Breast cancer: Basic Clin Res. 2020;14:p1178223420980377.
2. Mieog J, Van der Hage J, Van De Velde C. Neoadjuvant chemotherapy for operable breast cancer. J Br Surg. 2007;94(10):1189–200.
3. Redden MH, Fuhrman GM. Neoadjuvant chemotherapy in the treatment of breast cancer. Surg Clin. 2013;93(2):493–9.
4. Killelea BK, et al. Neoadjuvant chemotherapy for breast cancer increases the rate of breast conservation: results from the National Cancer Database. J Am Coll Surg. 2015;220(6):1063–9.
5. Charfare H, Limongelli S, Purushotham A. Neoadjuvant chemotherapy in breast cancer. J Br Surg. 2005;92(1):14–23.
6. Schott AF, Hayes DF. *Defining the benefits of neoadjuvant chemotherapy for breast cancer*. 2012, American Society of Clinical Oncology. pp. 1747–1749.
7. Skarping I, et al. Neoadjuvant breast cancer treatment response; tumor size evaluation through different conventional imaging modalities in the NeoDense study. Acta Oncol. 2020;59(12):1528–37.

8. Romeo V, et al. Assessment and prediction of response to neoadjuvant chemotherapy in breast cancer: a comparison of imaging modalities and future perspectives. Cancers. 2021;13(14):3521.
9. Lin L, et al. Photoacoustic computed tomography of breast cancer in response to neoadjuvant chemotherapy. Adv Sci. 2021;8(7):2003396.
10. Baumgartner A, et al. Ultrasound-based prediction of pathologic response to neoadjuvant chemotherapy in breast cancer patients. Breast. 2018;39:19–23.
11. Kumar A, et al. Color Doppler ultrasonography for treatment response prediction and evaluation in breast cancer. Future Oncol. 2010;6(8):1265–78.
12. Zhou S-C, et al. The role of contrast-enhanced ultrasound in the diagnosis and pathologic response prediction in breast cancer: a meta-analysis and systematic review. Clin Breast Cancer. 2020;20(4):e490–509.
13. Jing H, et al. Early evaluation of relative changes in tumor stiffness by shear wave elastography predicts the response to neoadjuvant chemotherapy in patients with breast cancer. J Ultrasound Med. 2016;35(8):1619–27.
14. Gu J, et al. Early assessment of shear wave elastography parameters foresees the response to neoadjuvant chemotherapy in patients with invasive breast cancer. Breast Cancer Res. 2021;23(1):52.
15. Folkman J, et al. Isolation of a tumor factor responsible for angiogenesis. J Exp Med. 1971;133(2):275.
16. Makris A, et al. Reduction in angiogenesis after neoadjuvant chemoendocrine therapy in patients with operable breast carcinoma. Cancer: Interdisciplinary Int J Am Cancer Soc. 1999;85(9):1996–2000.
17. Kuo W-H, et al. Vascularity change and tumor response to neoadjuvant chemotherapy for advanced breast cancer. Ultrasound Med Biol. 2008;34(6):857–66.
18. Demené C, et al. Ultrafast Doppler reveals the mapping of cerebral vascular resistivity in neonates. J Cereb Blood Flow Metabolism. 2014;34(6):1009–17.
19. Ternifi R et al. Ultrasound high-definition microvasculature imaging with novel quantitative biomarkers improves breast cancer detection accuracy. Eur Radiol, 2022; 32(11):7448-7462
20. Bayat M, Fatemi M, Alizad A. Background removal and vessel filtering of noncontrast ultrasound images of microvasculature. IEEE Trans Biomed Eng. 2018;66(3):831–42.
21. Ghavami S, et al. Quantification of morphological features in non-contrast-enhanced ultrasound microvasculature imaging. IEEE Access. 2020;8:18925–37.
22. Ternifi R, et al. Quantitative biomarkers for cancer detection using contrast-free ultrasound high-definition microvessel imaging: fractal dimension, murray's deviation, bifurcation angle & spatial vascularity pattern. IEEE Trans Med Imaging. 2021;40(12):3891–900.
23. Gu J, et al. Hybrid high-definition microvessel imaging/shear wave elastography improves breast lesion characterization. Breast Cancer Res. 2022;24(1):1–13.
24. Adusei SA, et al. Quantitative biomarkers derived from a novel, Contrast-Free Ultrasound, High-Definition Microvessel Imaging for differentiating Choroidal tumors. Cancers. 2024;16(2):395.
25. Ferroni G, et al. Noninvasive prediction of axillary lymph node breast cancer metastasis using morphometric analysis of nodal tumor microvessels in a contrast-free ultrasound approach. Breast Cancer Res. 2023;25(1):65.
26. Kurti M, et al. Quantitative biomarkers derived from a novel contrast-free ultrasound high-definition microvessel imaging for distinguishing thyroid nodules. Cancers. 2023;15(6):1888.
27. Sabeti S, et al. Morphometric analysis of tumor microvessels for detection of hepatocellular carcinoma using contrast-free ultrasound imaging: a feasibility study. Front Oncol. 2023;13:1121664.
28. Gu J, et al. Volumetric imaging and morphometric analysis of breast tumor angiogenesis using a new contrast-free ultrasound technique: a feasibility study. Breast Cancer Res. 2022;24(1):85.
29. Shia WC, et al. Using Flow characteristics in three-Dimensional Power Doppler Ultrasound Imaging to predict complete responses in patients undergoing Neoadjuvant Chemotherapy. J Ultrasound Med. 2017;36(5):887–900.
30. Qi J, et al. The potential role of combined shear wave elastography and superb microvascular imaging for early prediction the pathological response to neoadjuvant chemotherapy in breast cancer. Front Oncol. 2023;13:1176141.
31. Lee EJ, Chang Y-W. Prediction of complete response after neoadjuvant chemotherapy for invasive breast cancers: the utility of shear wave elastography and superb microvascular imaging in pretreatment breast ultrasound. Eur J Radiol. 2024;175:111432.
32. Symmans WF, et al. Measurement of residual breast cancer burden to predict survival after neoadjuvant chemotherapy. J Clin Oncol. 2007;25(28):4414–22.
33. Hylton NM et al. Locally advanced breast cancer: MR imaging for prediction of response to neoadjuvant chemotherapy—results from ACRIN 6657/I-SPY TRIAL. Radiology, 2012. 263(3): pp. 663–72.
34. Luengo-Gil G, et al. Effects of conventional neoadjuvant chemotherapy for breast cancer on tumor angiogenesis. Breast Cancer Res Treat. 2015;151:577–87.
35. Mo T, et al. MRI Assessment of changes in Tumor Vascularization during Neoadjuvant anti-angiogenic treatment in locally advanced breast Cancer patients. Cancers. 2023;15(18):4662.

Publisher's note